*Published:* 2D Mater. **6**(1):Art. No. 015003 (2019)
DOI:10.1088/2053-1583/aae45c

# Spatially Selective Charge Carrier Density Tuning in $WS_2$ Monolayers via Photochlorination

*I. Demeridou[1,2], I. Paradisanos[1,2], C. L. Yuanyue[3], N. Pliatsikas[4], P. Patsalas[4], S.* Germanis[1], N. *Pelekanos[1,5], W. A. Goddard III[3], G. Kioseoglou[1,5]*, E. Stratakis[1,2]**

[1] Institute of Electronic Structure and Laser, Foundation for Research and Technology - Hellas, Heraklion, 71110, Crete, Greece

[2] Department of Physics, University of Crete, Heraklion, 71003, Crete, Greece

[3] Materials and Process Simulation Center, California Institute of Technology, Pasadena CA, 91125, USA

[4] Physics Department, Aristotle University of Thessaloniki, Thessaloniki, 54124, Greece

[5] Department of Materials Science and Technology, University of Crete, Heraklion, 71003 Crete, Greece

KEYWORDS: 2D Materials, Transition Metal Dichalcogenides, Tungsten Disulfide, Doping, Photochemical Chlorination, Exciton Binding Energy.

ABSTRACT

Chlorine-doped tungsten disulfide monolayer (1L-$WS_2$) with tunable charge carrier concentration has been realized by pulsed laser irradiation of the atomically thin lattice in a precursor gas atmosphere. This process gives rise to a systematic shift of the neutral exciton peak towards lower energies, indicating reduction of the crystal's electron density. The capability to progressively tune the carrier density upon variation of the exposure time is demonstrated; this implicates that the Fermi level shift is directly correlated to the respective electron density modulation due to the chlorine species. Notably, this electron withdrawing process enabled the determination of the trion binding energy of the intrinsic crystal, found to be as low as 20 meV, in accordance to theoretical predictions. At the same time, it is found that the effect can be reversed upon continuous wave laser scanning of the monolayer in air. Scanning Auger Microscopy and X-ray photoelectron spectroscopy are used to link the actual charge carrier doping to the different chlorine configurations in the monolayer lattice. The spectroscopic analyses, complemented by density functional theory calculations, reveal that chlorine physisorption is responsible for the carrier density modulation induced by the pulsed laser photochemical reaction process. Such bidirectional control of the Fermi level, coupled with the capability offered by lasers to process at pre-selected locations, can be advantageously used for spatially resolved doping modulation in 1L-$WS_2$ with micrometric resolution. This method can also be extended for the controllable doping of other TMD monolayers.

Monolayer (1L) transition metal dichalcogenides (TMDs) are promising materials for future 2D nanoelectronics due to their unique electrical,[1] optical[2,3] and mechanical properties.[4] Indeed, TMDs have been demonstrated to be ideal candidates for field-effect transistors, photovoltaic cells, light-emitting diodes, single-atom storage, molecule sensing, quantum-state metamaterials and electrocatalytic water splitting applications.[5–7]

Carrier modulation is an important parameter in the study of the electronic properties of semiconductors and at the heart of many applications in microelectronics. Tuning the charge carrier density, i.e. doping, can be realized chemically, via bonding of foreign atoms to the crystal structure,[8–10] or electrostatically, by inducing a charge accumulation.[11–13] Electrical doping

measurements of 1L $MoSe_2$[14] and $WSe_2$[15] have shown the tunability in the photoluminescence (PL) emission of the neutral (X) and negatively ($X^-$) or positively ($X^+$) charged excitons (so-called trions). Moreover, electrically tunable PL emission between $X^-$ and X components has been observed in $MoS_2$ and $WS_2$.[11,16] At the same time, chemical doping via the absorption of atoms in gas phase and organic molecules has been demonstrated to be a promising approach to tune the carrier density in TMDs.[12,17–21] Despite the numerous studies on TMDs' doping, reported to date, the fine control in charge carrier tunability, as well as the doping reversibility still remain unresolved issues.

In this Letter, we demonstrate the reversible tunability of the position of the neutral exciton emission peak of 1L-$WS_2$ via photoinduced chlorination of the atomically thin lattice. It is found that this is a consequence of the adsorption of electron withdrawing chlorine adatoms that strongly suppresses the electron concentration and enhances the PL efficiency. Theoretical calculations indicate that the charge transfer between the dopant species and the monolayer induces a shift in the Fermi level, giving rise to the observed modulation of the optical properties. Notably, it is found that the lattice can be driven back to its pristine state upon continuous wave (CW) laser induced removal of chlorine dopants. It is concluded that photo-assisted chemical doping provides a useful and fast tool for bidirectional control of the Fermi level in 1L-$WS_2$. More important, it enables, on-demand, spatially resolved doping modulation, upon laser induced adsorption/desorption in preselected locations, in a write-erase manner.

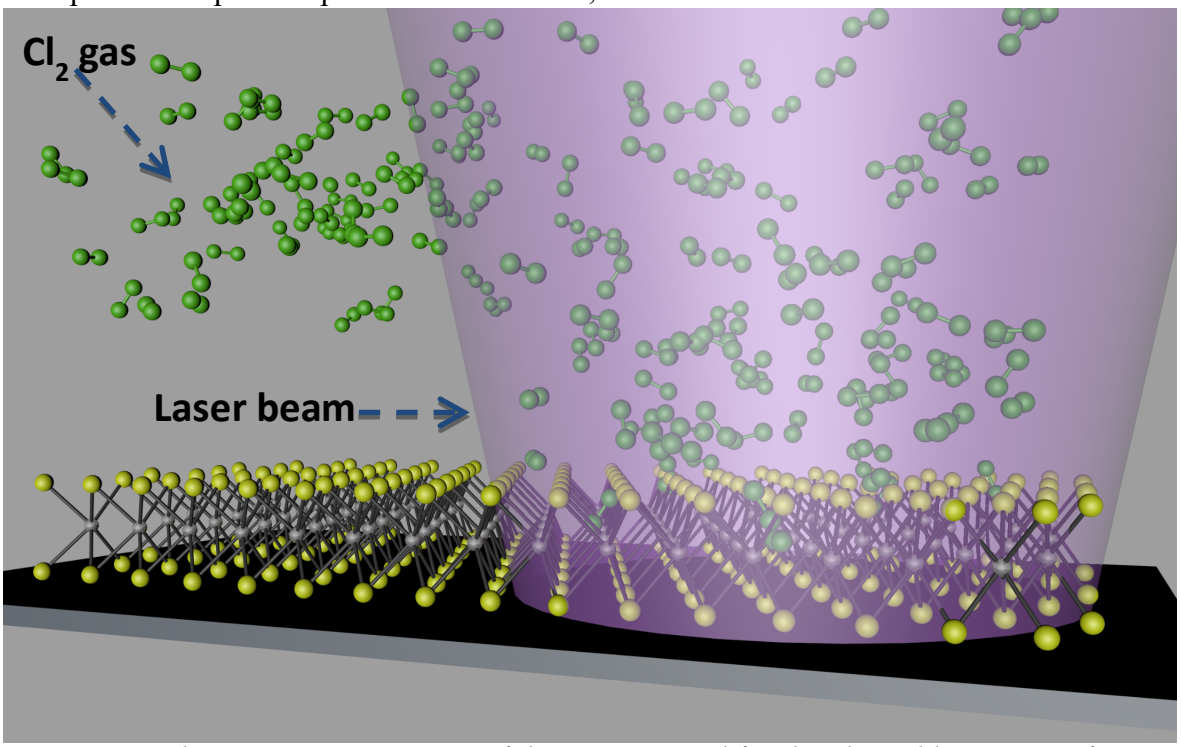


**Scheme 1**: *Schematic representation of the process used for the photochlorination of TMDs.*

$WS_2$ samples were mechanically exfoliated from a bulk crystal (2D semiconductors) using an adhesive tape and were subsequently placed onto 290 nm-thick $SiO_2$/Si substrates. Monolayer regions were identified via optical microscopy and confirmed with micro-Raman spectroscopy (Figure 1S) with very low laser power in order to avoid structural damage. The energy difference between the two main Raman vibrational modes, E′ (in plane mode) and $A_1$′ (out of plane mode), is used extensively in the literature as the fingerprint of the number of layers.[22]

Following exfoliation, the $WS_2$ monolayers were exposed to the irradiation of a 248 nm UV laser source emitting 20 ns pulses (ScheMateme 1) at a repetition rate of 1Hz. The whole process took place into a 120 Torr $Cl_2$ residual gas pressure. Different combinations of laser power (P) and number of pulses ($N_p$) were tested in an effort to optimize this photochlorination process. In a typical experiment, the sample was irradiated at a constant P with $N_p$ = 1, 5, 10, 20, 30 and 40 pulses, corresponding to photoreaction times of 1, 5, 10, 20, 30, and 40 s respectively.

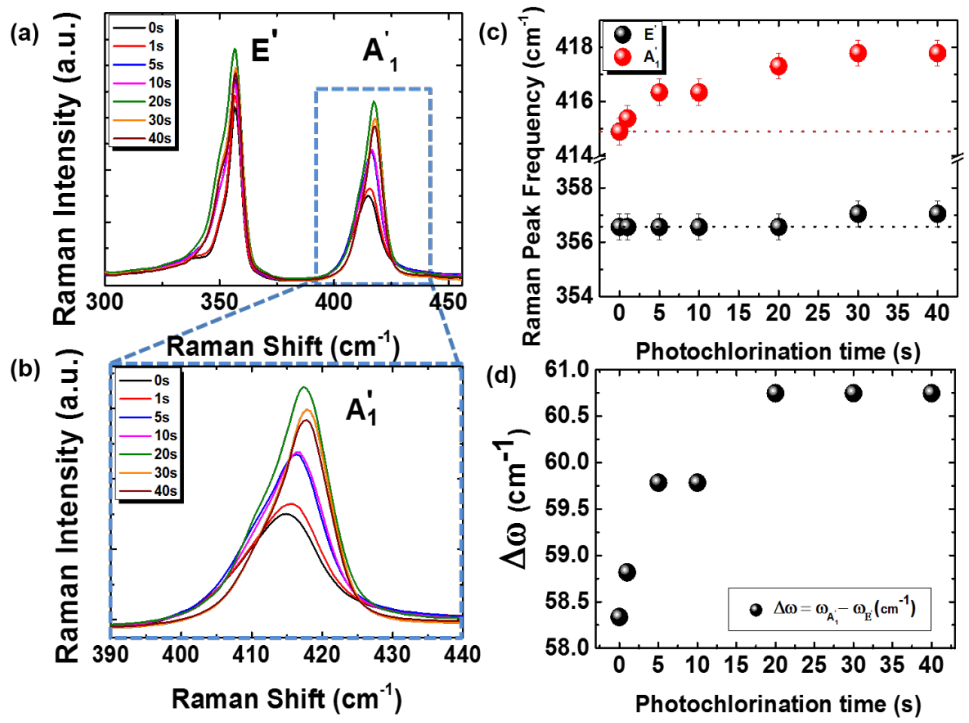


**Figure 1:** *(a) Evolution of the Raman Spectra of $WS_2$ monolayer with the photochlorination time shown in the inset. (c) Dependence of the $E'$ and the $A_1'$ peak frequencies on the photochlorination time. (b) Evolution of the out-of-plane vibrational mode $A_1'$. (d) Frequency separation between the $E'$ and the $A_1'$ modes as a function of the photochlorination time.*

Figure 1a presents the evolution of the micro-Raman spectrum of a 1L-$WS_2$, subjected to UV irradiation in $Cl_2$ environment, upon increasing the exposure time. The corresponding dependence of the E′ and $A_1'$ peak frequencies with doping steps is shown in Figure 1b. It is found that the $A_1'$ mode progressively blue-shifts upon irradiation for 40s in $Cl_2$, while the peak position of the E' mode remains unaffected. It is well reported that, in a typical 1L TMD, the out-of-plane mode, $A_1'$ is sensitive to charging effects due to the strong electron phonon coupling.[23,24] In particular, the observed blue shift of the $A_1'$ peak complies with electron withdrawing, i.e. p-type, doping. On the contrary, it is demonstrated that the in-plane, E', mode is not significantly influenced by electron doping.[19,23,24] Figure 1d shows the corresponding increase of the Raman frequency difference ($\Delta\omega = \omega(A_1')-\omega(E')$) with the doping time, which remains always within the reported limit of the monolayer energy difference of 59-61 $cm^{-1}$.[22,25] All above observations indicate a hole doping effect induced upon such photochlorination treatment.

Micro-PL spectroscopy and reflectivity measurements were used to further explore the hole doping effect induced by photochlorination. Figure 2a shows the PL spectra of monolayer $WS_2$ at 78 K at different photochlorination times. For the analysis of the different emission peaks, we fit the spectra with Gaussian functions acquiring high values of coefficient of determination ($R^2$>0.99).

The corresponding PL spectra were deconvoluted into three peaks (Figure 2b), which are assigned (from higher to lower energy) to neutral exciton (X) at 2.085eV, negatively charged exciton (trion, $X^-$) at 2.045eV, which arise from direct optical transitions at the K point and emission from biexcitons and localized states (XX/L).[26–28] Notably, the $X^-$ and X emission behave differently as a function of the photochlorination time. A first finding is that the X emission intensity is remarkably enhanced at the expense of the $X^-$ which can be explained as follows: $WS_2$ is a well-known n-type 2D material and its PL spectrum is accompanied by negatively charged trions even at room temperature.[27] Under the photochlorination treatment the electron concentration is reduced, suppressing the oscillator strength of the negatively charged trions and leading the PL spectral weight towards the neutral exciton emission.

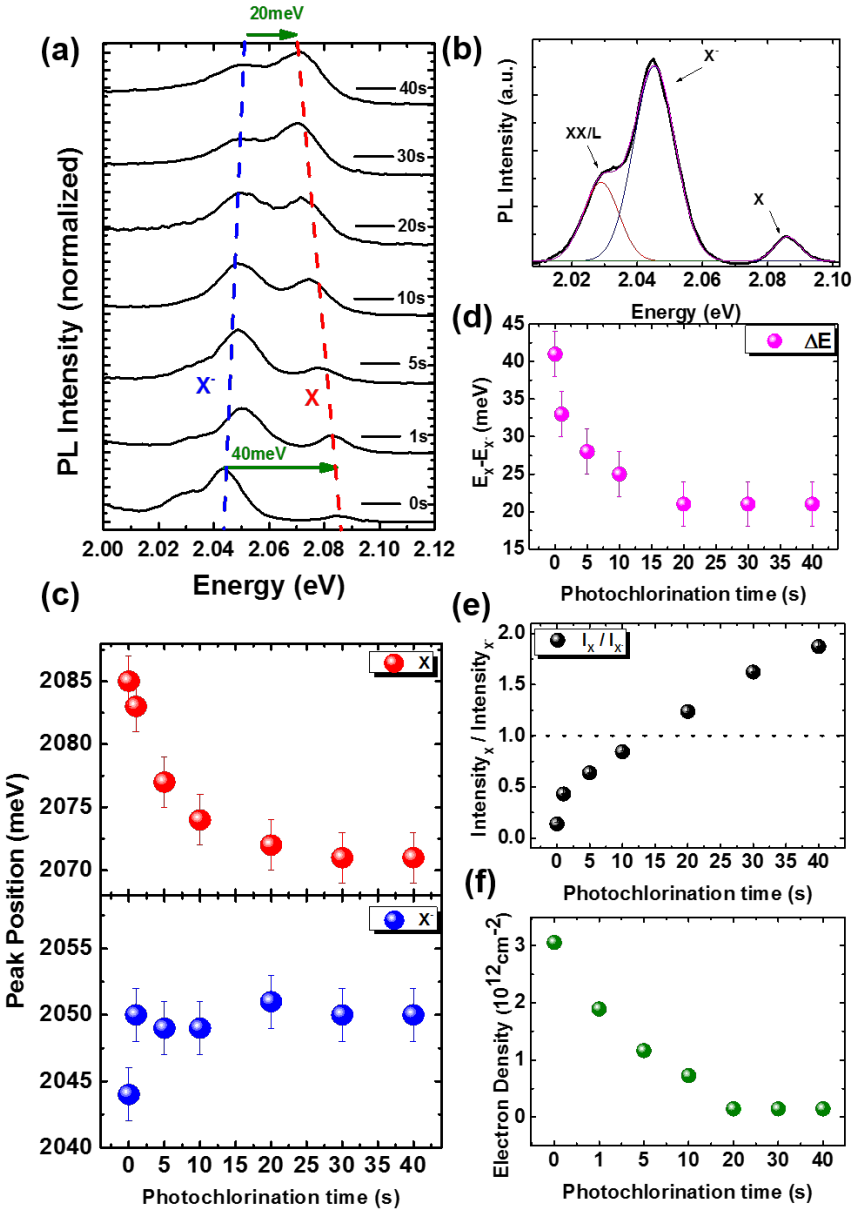


**Figure 2:** *(a) Evolution of the PL spectra of a 1L-$WS_2$ at 78K, with the photochlorination time. (b) Deconvolution of the initial PL spectrum obtained prior to the photochlorination process; the neutral exciton (X), negatively charged exciton (trion, $X^-$) and emission from localized states*

*(XX/L) peaks are assigned. (c) Peak position of X and $X^-$ as a function of the photochlorination time. (d) Dependence of the trion binding energy, corresponding to the energy difference between the X and $X^-$ peaks, on the photochlorination time. (e) The ratio of normalized intensities of the X and $X^-$ peaks as a function of the photochlorination time. (e) Evolution of the calculated electron density with the photochlorination time.*

More importantly, the X peak progressively redshifts with photochlorination time and tends to saturate at elevated exposure times (Figure 2c); On the other hand, the $X^-$ peak weakly blueshifts (Figure 2c). As a result, the trion binding energy, corresponding to the energy difference between the X and $X^-$, decreases with the photochlorination time (Figure 2d), in agreement to previous reports on electron doping in 1L-$WS_2$, 1L-$MoS_2$ and 1L-$WSe_2$.[11,19] Such reduction in the trion binding energy can be attributed to the Fermi level lowering upon photochemical doping with chlorine. It is interesting also that the trion binding energy saturates to the quite low value of ~20meV, which is in agreement to theoretical predictions for the 1L-$WS_2$ intrinsic (undoped) crystal.[29] The observations will be further discussed in the DFT calculations section below. Figure 2e shows the ratio of normalized intensities of two excitonic components as a function of the doping steps. The as-exfoliated 1L-$WS_2$ is of n-type and thus rich in electrons, which enhances the probability of $X^-$ formation; as a result the spectral weight of the $X^-$ peak is initially predominant. The progressive suppression of the $X^-$ peak, coupled with the monotonical enhancement of the X peak observed upon photochlorination can be interpreted as a reduction of the 1L-$WS_2$ electron density, which can be also attributed to the Fermi level lowering. The corresponding splitting between the exciton ($\omega_x$) and trion energy ($\omega_x^-$) is predicted to be linearly dependent on the Fermi energy[11] and obey the equation: $\omega_x - \omega_x^- = E_b + E_F$. Based on this equation, the electron density $n_e$ can be calculated (see Supporting Information), assuming the measured $E_b$ of 20 meV and the effective mass of electrons as $m_e=0.35m_0$[11,35] where $m_0$ is the free electron mass. The calculated electron density $n_e$ as a function of the photochlorination time is shown in Figure 2f; the electron densities of 1L-$WS_2$ before and after doping in the saturation region are $\sim 3.05 \times 10^{12}$ and $\sim 0.14 \times 10^{12}$ $cm^{-2}$, respectively, while their difference is $\Delta n_e \sim 2.91 \times 10^{12}$ $cm^{-2}$. The capability to progressively tune the carrier density upon variation of the photochlorination time, shown in Figure 2e, implicates that the Fermi level shift can be directly correlated to the respective electron density modulation due to the chlorine species.

Differential reflectivity measurements performed in the same 1L-$WS_2$ (Figure 2S, supporting information) are in remarkable agreement with the micro-PL results described above. The respective spectra show again the two distinct excitonic absorption peaks, $X^-$ and X, at ~2.04eV and ~2.086eV respectively.[26] Moreover, the $X^-$ absorption, in differential spectra, was suppressed by doping, while the trion binding energy saturates to the same value of ~20 meV (Figure 2Sa), in accordance to the results obtained by the micro-PL spectra.

To shed light on the photoinduced reaction process between 1L-$WS_2$ and $Cl_2$, topographic X-Ray Photoelectron Spectroscopy (XPS) and Scanning Auger Microscopy (SAM) were used to determine the chemical state of the W, S and Cl. In a first step the XPS spectra of single $WS_2$ layers before and after the photochlorination treatment were compared, as presented in Figure 3a. Notably, in the spectrum of the photochlorinated sample a characteristic Cl peak was detected, in addition to the photoelectron lines of W, S, adventitious C and Si (due to the substrate) observed in the pristine sample. The corresponding [S]/[W] ratio, however, was remained close to 2 showing that there is no significant replacement of S with Cl. On the other hand, SAM detected no Cl on the surface of the laser-treated sample, suggesting that Cl is loosely bonded on $WS_2$ and that desorption of chlorine species from $WS_2$, due to the heating of the surface by the high energy/high

flux electron beam, takes place. More detailed information on the chemical bonding can be deduced from analyzing the XPS core-level spectra of the constituent elements. Figure 3b and 3c show the S-*2p* and the W-*4f* core level spectra, respectively, for the two samples (pristine and Cl-doped). In both lines the split due to spin-orbit coupling is observed, so the core level spectra consist of doublets (S-$2p^{1/2}$ and S-$2p^{3/2}$ as well as W-$4f^{5/2}$ and W-$4f^{7/2}$).

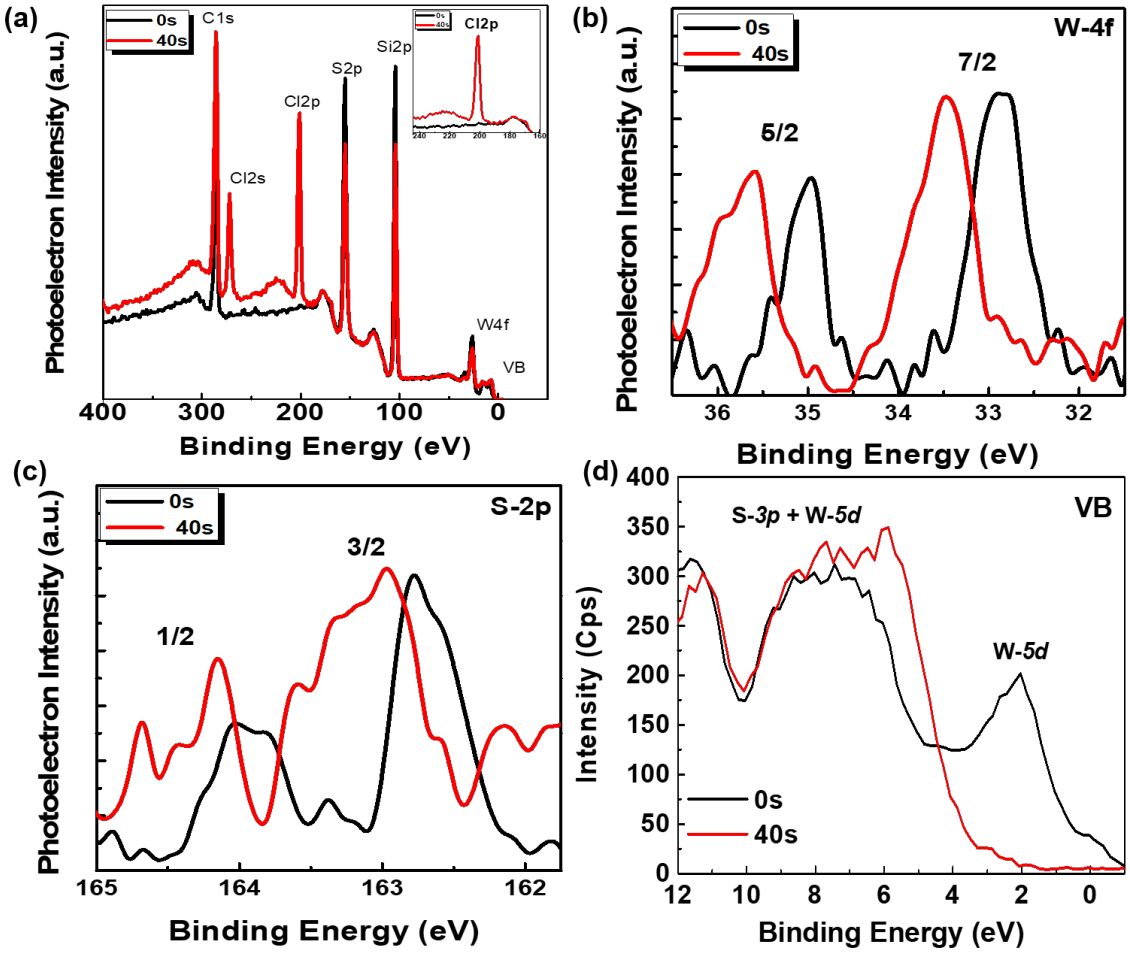


**Figure 3:** *(a) XPS wide scan spectra of the pristine (black curve) and photochlorinated for 40s (red curve) 1L-$WS_2$. The legends indicate the assignment of the corresponding photoelectron peaks; Corresponding W-4f (b) and S-2p (c) core level spectra, showing splitting due to spin-orbit coupling; (d) Corresponding valence band spectra of the 1L-$WS_2$ samples.*

In the case of W-4*f* core level spectra, the binding energy of the W-$4f^{7/2}$ is observed to be that of pure $WS_2$,[30] thus proving the quality of this reference sample. In the case of the sample exposed to Cl, the dominant W-$4f^{7/2}$ peak is located at higher binding energy, indicating a charge transfer due to Cl incorporation, which is also observed for W-Cl bonds in $WCl_4$.[31] Further insight is provided by analyzing the S-$2p^{3/2}$ core-level spectra (Figure 3d). Indeed the S-$2p^{3/2}$ peak for the pristine $WS_2$ is detected at the expected binding energy for pure $WS_2$.[30] In the case of the Cl-doped sample there is both a shift of the S-*2p* doublet, from the 162.8 eV for pure $WS_2$, and a fine structure of the S-$2p^{3/2}$ peak with contributions at 163.1 and 163.5 eV. The former can be attributed to S-containing aromatic compounds, such as thiophenol[32] which might be formed on the surface of the samples

by reaction of the adventitious carbon with S in the presence of Cl upon laser irradiation; the latter might be attributed to either S-containing aliphatic compounds,[32] formed on the surface of the samples by reaction of the adventitious carbon with S in the presence of Cl upon laser irradiation, or to S-Cl bonds similar to those observed in disulfur dichloride ($S_2Cl_2$).[32] All of the aforementioned compounds (e.g. thiophenol, and $S_2Cl_2$) decompose or desorb upon annealing at mild temperatures (e.g. 137 °C for $S_2Cl_2$),[33] while even W chlorides decompose and desorb upon electron irradiation[34] ; this explains the lack of detection of Cl in SAM experiments due to the heating of the sample's surface by the incoming electron beam. As a conclusion, Cl seems to develop Cl-S bonds mostly with the S atomic layer, which result in charge transfer from W, as well, due to the high electronegativity of Cl.

To gain a deeper understanding of the chemical bonding attained due to photochlorination reactions, spin-polarized Density Functional Theory (DFT) calculations, were carried out. Two different scenarios for the interaction of chlorine with 1L-$WS_2$ have been investigated, namely chlorine atoms are filling S vacancies or become adsorbed on a basal plane. The DFT calculation revealed that in the former bonding configuration, chlorine creates a donor level in 1L-$WS_2$ (Figure 4a), giving rise to a Fermi level shift towards the conduction band and therefore cannot account for the observed red shift of the neutral exciton peak. On the contrary, chlorine adsorption creates an acceptor level, which likely shifts down the Fermi level of n-type $WS_2$ (Figure 4b) and therefore complies with the neutral exciton peak red shift. The chlorine desorption effect revealed by the DFT calculations complies with the XPS findings discussed above.

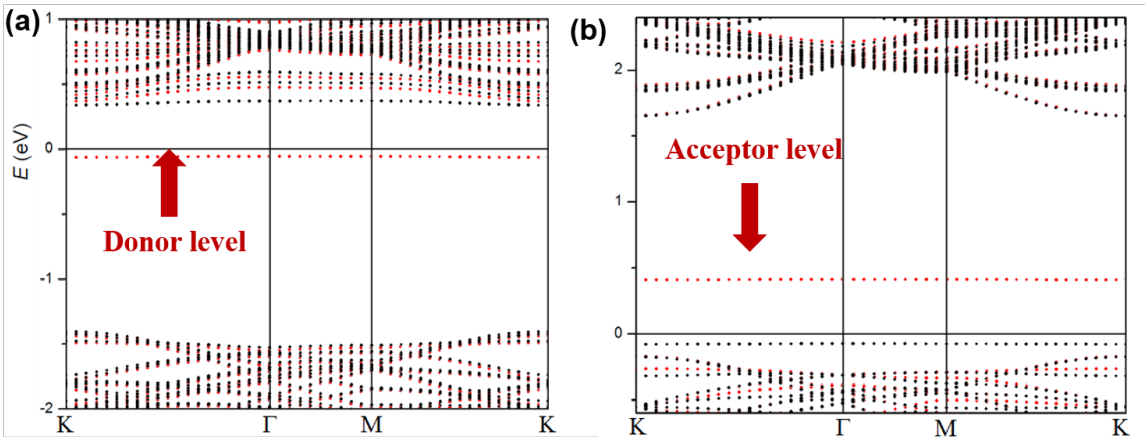


**Figure 4:** *Spin-polarized Density Functional Theory calculations of the photochlorination reaction process in 1L-$WS_2$: (a) Simulation of Chlorine atoms filling S vacancies; (b) Simulation of Chlorine atoms adsorbed on the basal plane.*

We find that the observed photochlorination effect can be reversed upon CW laser (473nm) rastering of the chlorine-doped 1L-$WS_2$, possibly due to the laser induced desorption of chlorine atoms from the monolayer. In particular, following such a dechlorination process, the Raman $A_1'$ mode position, the PL intensity as well as the trion binding energy, return practically back to the levels prior to photochlorination (Figure 5 and Figure 3S and 4S). The respective micro-PL and differential reflectance spectra are presented in Figure 5. As shown in this Figure, both the PL and reflectivity spectra evolve upon increasing the CW laser power from 3.16kW/cm$^2$ to 3.56kW/cm$^2$, but become stable upon further increasing the CW power. It is also found that the degree of dechlorination can be also controlled with the variation of the rastering time. Based on the above observations, we can postulate that the photochlorination approach, demonstrated here, provides a

useful tool for bidirectional (extraction or injection of electrons) control of the electron density levels in 1L-$WS_2$.

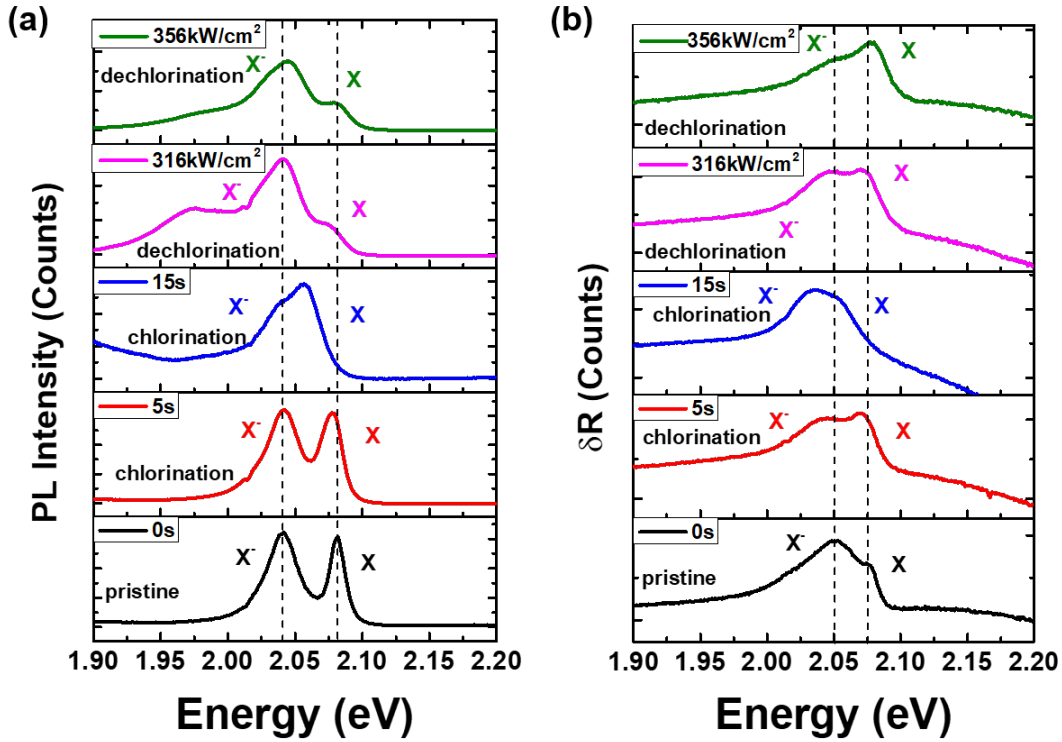


**Figure 5:** *PL (a) and differential reflectance (b) spectra of a pristine 1L-$WS_2$ (black curves) and photochlorinated for 5s (red curves) and 15s (blue curves) respectively. The corresponding spectra obtained after CW laser rastering of the monolayer area using 316 kW/cm² (magenta curves) and 356 kW/cm² (green curves) are also presented. The resonant energies the X and $X^-$ excitons are indicated with dotted lines.*

The above results indicate the possibility of a laser induced chlorination/dechlorination process enabling spatially selective doping changes with a beam size, i.e. micrometer, resolution. As a proof of this concept, we have exposed part of a pristine (Figure 6a) $WS_2$ monolayer to UV pulses in chlorine (Figure 6b) and subsequently we scanned the same area with a 473nm CW laser beam in air (Figure 6c). Figure 6d shows the respective normalized-intensity PL spectra, indicating the reversibility of the photochlorination effect. Furthermore, due to the spatial control of photochlorination we oberve a much stronger PL emission by the photochlorinated area (area B in Figure 6b and magenta curve in Figure 6d) compared to the pristine one (area A in Figure 6b and blue curve in Figure 6d), which is restored back to the levels of the monolayer in its pristine state upon CW laser cleaning (area C in Figure 6c and green curve in Figure 6d). This light-induced bidirectional doping process could potentially provide erasable regions of customized doping levels or even the formation of in-plane electronic junctions.

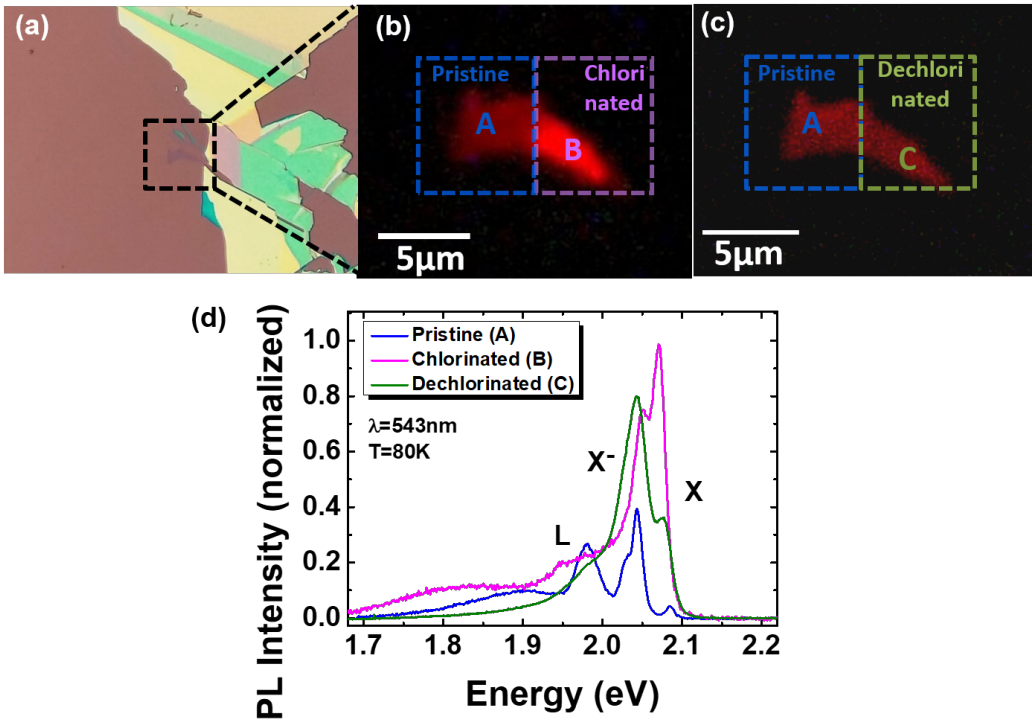


**Figure 6.** *(a) Optical microscopy image of an exfoliated 1L-$WS_2$. (b) Fluorescence image of the monolayer following selective photochlorination of the area assigned as B, as indicated by the stronger PL emission compared to the area denoted as A. (c) Reversal of the photochlorination effect upon CW laser rastering of the chlorine-doped area, indicated by the suppresion of the PL emission by the area assigned as C (d) The corresponding PL spectra of the pristine1L-$WS_2$ (blue curve), photochlorinated (magenta curve) and dechlorinated (green curve) areas.*

In summary, we have demonstrated the spatially resolved and reversible tuning of the PL properties of 1L-$WS_2$ using a pulsed laser photodoping process. It is shown that the PL intensity can be significantly enhanced via the photo-assisted adsorption of p-type chlorine dopants to the monolayer lattice. This is due to the switching of the dominant PL process from the recombination of negative trions to that of neutral excitons, under the annihilation of residual electrons from the pristine crystal. DFT calculations confirm that chlorine adsorption can significantly affect the lattice electron density resulting in considerable shifts in the Fermi level position and to complete charge neutralization. Another remarkable finding is that the doping effect can be gradually reversed upon CW laser removal of the adsorbed chlorine species. This all-optical, bidirectional tuning of the electron density developed here can be advantageously used for spatially resolved doping modulation in 1L-$WS_2$ with micrometric resolution. It can therefore be important for the fabrication of TMD-based light-emitting and photovoltaic devices as well as in reducing the contact resistance between the TMD channel and the metal electrodes in field effect transistors. Although in the present study we have introduced a photochemical chlorination method to control the carrier density in 1L-$WS_2$, this process can be readily extended to alternate combinations of dopants and TMD materials.

**Experimental Methods**

*Sample preparation:* $WS_2$ samples were mechanically exfoliated from a bulk crystal (HQ Graphene) using an adhesive tape and were subsequently placed onto n-doped Si wafers covered by a 285nm thick $SiO_2$ layer.
*Photochlorination process:* The as-prepared $WS_2$ monolayers were subjected to irradiation by a KrF excimer UV laser beam emitting 20 ns pulses of 248 nm at 1Hz repetition rate that was translated onto the monolayer area. For uniform exposure to laser radiation, a top-flat beam profile of 20×10 $mm^2$ was obtained using a beam homogenizer. The whole process took place into a vacuum chamber at 120 Torr $Cl_2$ gas pressure maintained through a precision micro valve system. Different combinations of laser power (P) and number of pulses ($N_p$) were tested in an effort to optimize the photochlorination process. In a typical experiment, the sample was irradiated at a constant P with $N_p$ = 1, 5, 10, 20, 30 and 40 pulses, corresponding to different photoreaction times equal to 1, 5, 10, 20, 30 and 40 s.
*Optical Spectroscopy:* For optical spectroscopy measurements we used a combined micro-Reflectivity/μ-PL setup. A Mitutoyo 50x (NA:0.42, *f*=200mm) lens was used to focus the excitation beam, down to ~1μm size, onto the sample, which is placed inside continuous-flow cryostat (ST500, Jannis). The position of the sample is controlled with a XYZ mechanical translation stage (PT3, Thorlabs) and the excitation procedure is continuously monitored and controlled via a CCD optical setup. Following the excitation, the emitted PL signal passes through a long pass filter to eliminate the emission of the laser. The same optical setup can be easily modified by flipping the mirrors of the μPL configuration, allowing the aligned super continuum light (360nm - 2600nm) of a stabilized tungsten-halogen source (SL201L, Thorlabs), to pass through an iris and follow the same optical path. The diameter of the white light spot size on the sample was approximately 3μm. In a typical experiment, the electronic transitions of 1L-$WS_2$ were probed with the broadband light and the reflected signal that follows the backscattering geometry was measured. However, because the flakes are atomically thin and placed on $SiO_2$/Si substrate, the reflected light spectra included the illumination source profile, the sample transmission and absorption, the substrate reflection and absorption, and resonant effects due to the thickness of the $SiO_2$. To distinguish the contribution from the 1L-$WS_2$, we take the difference between the intensity measured from the monolayer, $I_{on}$, and from the substrate just off the monolayer, $I_{off}$, and normalize to the intensity from the substrate, $\Delta R=(I_{on}-I_{off})/I_{off}$.
*Raman Spectroscopy:* Raman spectroscopy of the samples was performed, under 473 nm excitation in ambient conditions (Thermo Scientific). During measurements, the laser power was kept below 1 mW to avoid heating and thus possible damage the samples. The Raman emission was collected in a back scattering geometry, using a 100X objective at room temperature.
*X-ray Photoelectron (XPS) and Scanning Auger Microscopy (SAM):* The X-ray Photoelectron Spectra (XPS) and the Scanning Auger Microscopy (SAM) images were acquired in a KRATOS Axis Ultra DLD system equipped with a monochromated AlKa X-ray source, a Field Emission Gun (FEG), a hemispherical sector electron analyzer and a multichannel electron detector. The XPS measurements were acquired using 20 eV pass energy providing a full-width at half maximum (FWHM) less than 500 meV for the Ag-$3d^{5/2}$ peak. The spot size used to acquire the XPS spectra was 15 μm. External charging effects (due to emission of photoelectrons) were considered and excluded from the spectra using the C-*1s* peak of the adventitious Carbon on the surface of the samples.
FIGURES (Word Style "VA_Figure_Caption"). Each figure must have a caption that includes the figure number and a brief description, preferably one or two sentences. The caption should immediately follow the figure with the format "**Figure 1.** Figure caption." All figures must be

mentioned in the text consecutively and numbered with Arabic numerals. The caption should be understandable without reference to the text. It is preferable to place the keys to symbols used in the figure in the caption, not in the artwork. Ensure that the symbols and abbreviations in the caption agree with those in the figure itself and in the text and that the figure is already sized appropriately.

SCHEMES (Word Style "VC_Scheme_Title"). Chemical reactions and flow diagrams may be called schemes. Schemes may have brief titles describing their contents. The artwork for each scheme should immediately follow the scheme title. The title should follow the format "**Scheme 1.** Scheme Title". All schemes must be mentioned in the text consecutively and numbered with Arabic numerals. Schemes may also have footnotes (use Word Style "FD_Scheme_Footnote"), inserted after the artwork.

CHARTS (Word Style "VB_Chart_Title"). Lists of structures may be called charts. Charts may have brief titles describing their contents. The title should follow the format "**Chart 1.** Chart Title". Charts may also have footnotes (use Word Style "FC_Chart_Footnote"). To insert the chart into the template, be sure it is already sized appropriately and paste it immediately after the chart title.

TABLES. Each table must have a brief (one phrase or sentence) title that describes its contents. The title should follow the format "**Table 1.** Table Title" (Word Style "VD_Table_Title"). The title should be understandable without reference to the text. Put details in footnotes, not in the title (use Word Style "FE_Table_Footnote"). Define nonstandard abbreviations in footnotes. Use tables (Word Style "TC_Table_Body") when the data cannot be presented clearly as narrative, when many precise numbers must be presented, or when more meaningful interrelationships can be conveyed by the tabular format. Do not use Word Style "TC_Table_Body" for tables containing artwork. Tables should supplement, not duplicate, text and figures. Tables should be simple and concise. It is preferable to use the Table Tool in your word-processing package, placing one entry per cell, to generate tables.

**Displayed equations** can be inserted where desired making sure they are assigned Word Style "Normal". Displayed equations can only be one column wide. If the artwork needs to be two columns wide, it must be relabeled as a figure, chart, or scheme and mentioned as such in the text.

ASSOCIATED CONTENT

(Word Style "TE_Supporting_Information"). **Supporting Information**. A listing of the contents of each file supplied as Supporting Information should be included. For instructions on what should be included in the Supporting Information as well as how to prepare this material for publications, refer to the journal's Instructions for Authors.

The following files are available free of charge.

brief description (file type, i.e., PDF)

brief description (file type, i.e., PDF)

AUTHOR INFORMATION

**Corresponding Author**

*(Word Style "FA_Corresponding_Author_Footnote"). * (Word Style "FA_Corresponding_Author_Footnote"). Give contact information for the author(s) to whom correspondence should be addressed.

**Present Addresses**

†If an author's address is different than the one given in the affiliation line, this information may be included here.

**Author Contributions**
The manuscript was written through contributions of all authors. All authors have given approval to the final version of the manuscript. ‡These authors contributed equally. (match statement to author names with a symbol)
**Funding Sources**
Any funds used to support the research of the manuscript should be placed here (per journal style).
**Notes**
Any additional relevant notes should be placed here.
ACKNOWLEDGMENT
(Word Style "TD_Acknowledgments"). Generally the last paragraph of the paper is the place to acknowledge people, organizations, and financing (you may state grant numbers and sponsors here). Follow the journal's guidelines on what to include in the Acknowledgments section.
ABBREVIATIONS
CCR2, CC chemokine receptor 2; CCL2, CC chemokine ligand 2; CCR5, CC chemokine receptor 5; TLC, thin layer chromatography.

REFERENCES
(1) Novoselov, K. S.; Jiang, D.; Schedin, F.; Booth, T. J.; Khotkevich, V. V; Morozov, S. V; Geim, A. K. Two-Dimensional Atomic Crystals. *Proc. Natl. Acad. Sci. U. S. A.* **2005**, *102* (30), 10451–10453.
(2) Mak, K. F.; Lee, C.; Hone, J.; Shan, J.; Heinz, T. F. Atomically Thin MoS2: A New Direct-Gap Semiconductor. *Phys. Rev. Lett.* **2010**, *105* (13).
(3) Sundaram, R. S.; Engel, M.; Lombardo, A.; Krupke, R.; Ferrari, A. C.; Avouris, P.; Steiner, M. Electroluminescence in Single Layer MoS2. *Nano Lett.* **2013**, *13* (4), 1416–1421.
(4) Bertolazzi, S.; Brivio, J.; Kis, A. Stretching and Breaking of Ultrathin MoS 2. *ACS Nano* **2011**, *5* (12), 9703–9709.
(5) Petrone, N.; Hone, J.; Akinwande, D. Two-Dimensional Flexible Nanoelectronics. *Nat. Commun.* **2015**, *5*, 1–12.
(6) Wang, Q. H.; Kalantar-Zadeh, K.; Kis, A.; Coleman, J. N.; Strano, M. S. Electronics and Optoelectronics of Two-Dimensional Transition Metal Dichalcogenides. *Nat. Nanotechnol.* **2012**, *7* (11), 699–712.
(7) Perkins, F. K.; Friedman, A. L.; Cobas, E.; Campbell, P. M.; Jernigan, G. G.; Jonker, B. T. Chemical Vapor Sensing with Monolayer MoS2. *Nano Lett.* **2013**, *13* (2), 668–673.
(8) Saigal, N.; Wielert, I.; Čapeta, D.; Vujičić, N.; Senkovskiy, B. V.; Hell, M.; Kralj, M.; Grüneis, A. Effect of Lithium Doping on the Optical Properties of Monolayer MoS $_2$. *Appl. Phys. Lett.* **2018**, *112* (12), 121902.
(9) Howard, C. A.; Dean, M. P. M.; Withers, F. Phonons in Potassium-Doped Graphene: The Effects of Electron-Phonon Interactions, Dimensionality, and Adatom Ordering. *Phys. Rev. B - Condens. Matter Mater. Phys.* **2011**, *84* (24), 1–4.
(10) Dolui, K.; Rungger, I.; Das Pemmaraju, C.; Sanvito, S. Possible Doping Strategies for MoS2 Monolayers: An Ab Initio Study. *Phys. Rev. B - Condens. Matter Mater. Phys.* **2013**, *88* (7), 1–9.
(11) Mak, K. F.; He, K.; Lee, C.; Lee, G. H.; Hone, J.; Heinz, T. F.; Shan, J. Tightly Bound Trions in Monolayer MoS2. *Nat. Mater.* **2013**, *12* (3), 207–211.

(12) Tongay, S.; Zhou, J.; Ataca, C.; Liu, J.; Kang, J. S.; Matthews, T. S.; You, L.; Li, J.; Grossman, J. C.; Wu, J. Broad-Range Modulation of Light Emission in Two-Dimensional Semiconductors by Molecular Physisorption Gating. *Nano Lett.* **2013**, *13* (6), 2831–2836.
(13) Cho, K.; Park, W.; Park, J.; Jeong, H.; Jang, J.; Kim, T. Y.; Hong, W. K.; Hong, S.; Lee, T. Electric Stress-Induced Threshold Voltage Instability of Multilayer MoS2 Field Effect Transistors. *ACS Nano* **2013**, *7* (9), 7751–7758.
(14) Ross, J. S.; Wu, S.; Yu, H.; Ghimire, N. J.; Jones, A. M.; Aivazian, G.; Yan, J.; Mandrus, D. G.; Xiao, D.; Yao, W.; et al. Electrical Control of Neutral and Charged Excitons in a Monolayer Semiconductor. *Nat. Commun.* **2013**, *4*, 1474.
(15) Jones, A. M.; Yu, H.; Ghimire, N. J.; Wu, S.; Aivazian, G.; Ross, J. S.; Zhao, B.; Yan, J.; Mandrus, D. G.; Xiao, D.; et al. Optical Generation of Excitonic Valley Coherence in Monolayer WSe 2. *Nat. Nanotechnol.* **2013**, *8* (9), 634–638.
(16) Zhu, B.; Chen, X.; Cui, X. Exciton Binding Energy of Monolayer WS2. *Sci. Rep.* **2015**, *5* (1), 9218.
(17) Kim, E.; Ko, C.; Kim, K.; Chen, Y.; Suh, J.; Ryu, S. G.; Wu, K.; Meng, X.; Suslu, A.; Tongay, S.; et al. Site Selective Doping of Ultrathin Metal Dichalcogenides by Laser-Assisted Reaction. *Adv. Mater.* **2016**, *28* (2), 341–346.
(18) Kim, Y.; Jhon, Y. I.; Park, J.; Kim, C.; Lee, S.; Jhon, Y. M. Plasma Functionalization for Cyclic Transition between Neutral and Charged Excitons in Monolayer MoS2. *Sci. Rep.* **2016**, *6* (January), 1–10.
(19) Peimyoo, N.; Yang, W.; Shang, J.; Shen, X.; Wang, Y.; Yu, T. Chemically Driven Tunable Light Emission of Charged and Neutral Excitons in Monolayer WS2. *ACS Nano* **2014**, *8* (11), 11320–11329.
(20) Mouri, S.; Miyauchi, Y.; Matsuda, K. Tunable Photoluminescence of Monolayer $MoS_2$ via Chemical Doping. *Nano Lett.* **2013**, *13* (12), 5944–5948.
(21) Eda, G.; Yamaguchi, H.; Voiry, D.; Fujita, T.; Chen, M.; Chhowalla, M. Photoluminescence from Chemically Exfoliated MoS 2. *Nano Lett.* **2011**, *11* (12), 5111–5116.
(22) Zhao, W.; Ghorannevis, Z.; Amara, K.; Pang, J. Lattice Dynamics in Mono-and Few-Layer Sheets of WS2 and WSe2. *Nanoscale* **2013**, *5* (20), 9677–9683.
(23) Chakraborty, B.; Bera, A.; Muthu, D. V. S.; Bhowmick, S.; Waghmare, U. V; Sood, A. K. Symmetry-Dependent Phonon Renormalization in Monolayer MoS 2 Transistor. **2012**, *161403*, 2–5.
(24) Nan, H.; Wang, Z.; Wang, W.; Liang, Z.; Lu, Y.; Chen, Q.; He, D.; Tan, P.; Miao, F.; Wang, X.; et al. Strong Photoluminescence Enhancement of MoS 2 through Defect Engineering and Oxygen Bonding. **2014**, No. 6, 5738–5745.
(25) Paradisanos, I.; Pliatsikas, N.; Patsalas, P.; Fotakis, C.; Kymakis, E.; Kioseoglou, G.; Stratakis, E. Spatial Non-Uniformity in Exfoliated WS2 Single Layers. *Nanoscale* **2016**, *8*.
(26) Zhao, W.; Ghorannevis, Z.; Chu, L.; Toh, M.; Kloc, C.; Tan, P. H.; Eda, G. Evolution of Electronic Structure in Atomically Thin Sheets of WS2 and WSe2. *ACS Nano* **2013**, *7* (1), 791–797.
(27) Paradisanos, I.; Germanis, S.; Pelekanos, N. T.; Fotakis, C.; Kymakis, E.; Kioseoglou, G.; Stratakis, E. Room Temperature Observation of Biexcitons in Exfoliated $WS_2$ monolayers. *Appl. Phys. Lett.* **2017**, *110* (19).
(28) Plechinger, G.; Nagler, P.; Kraus, J.; Paradiso, N.; Strunk, C.; Schuller, C.; Korn, T. Identification of Excitons, Trions and Biexcitons in Single-Layer WS2. *Phys. Status Solidi - Rapid Res. Lett.* **2015**, *9* (8), 457–461.

(29) Bracker, A. S.; Stinaff, E. A.; Gammon, D.; Ware, M. E.; Tischler, J. G.; Park, D.; Gershoni, D.; Filinov, A. V.; Bonitz, M.; Peeters, F.; et al. Binding Energies of Positive and Negative Trions: From Quantum Wells to Quantum Dots. *Phys. Rev. B - Condens. Matter Mater. Phys.* **2005**, *72* (3), 1–6.
(30) Mccreary, K. M.; Hanbicki, A. T.; Jernigan, G. G.; Culbertson, J. C.; Jonker, B. T. Synthesis of Large-Area WS 2 Monolayers with Exceptional Photoluminescence. *Nat. Publ. Gr.* **2016**, No. August 2015, 1–7.
(31) Halada, G. P.; Clayton, C. R. Comparison of Mo – N and W – N Synergism during Passivation of Stainless Steel through Xray Photoelectron Spectroscopy and Electrochemical Analysis Comparison of Mo-N and W-N Synergism during Passivation of Stainless Steel through x-Ray Photoelectron Spec. **2014**, *2342* (1993).
(32) Search, H.; Journals, C.; Contact, A.; Iopscience, M. Molecular Spectroscopy by Means of ESCA. *286*.
(33) Williams, M. The Merck Index: An Encyclopedia of Chemicals, Drugs, and Biologicals, 15th Edition Edited by M.J.O'Neil, Royal Society of Chemistry, Cambridge, UK ISBN 9781849736701; 2708 Pages. April 2013, $150 with 1-Year Free Access to The Merck Index Online. *Drug Dev. Res.* **2013**, *74* (5), 339–339.
(34) Neustetter, M.; Da Silva, F. F.; Denifl, S. Electron Interactions with the Focused Electron Beam Induced Processing (FEBID) Precursor Tungsten Hexachloride. *Rapid Commun. Mass Spectrom.* **2016**, *30* (9), 1139–1144.
(35) Cheiwchanchamnangij, T.; Lambrecht, W. R. L. Quasiparticle Band Structure Calculation of Monolayer, Bilayer, and Bulk MoS2. *Phys. Rev. B - Condens. Matter Mater. Phys.* **2012**, *85* (20), 1–4.
(36) Ramasubramaniam, A. Large Excitonic Effects in Monolayers of Molybdenum and Tungsten Dichalcogenides. **2012**, *115409* (September), 1–6.

(Word Style "TF_References_Section"). References are placed at the end of the manuscript. Authors are responsible for the accuracy and completeness of all references. Examples of the recommended format for the various reference types can be found at http://pubs.acs.org/page/4authors/index.html. Detailed information on reference style can be found in *The ACS Style Guide,* available from Oxford Press.

BRIEFS (Word Style "BH_Briefs"). If you are submitting your paper to a journal that requires a brief, provide a one-sentence synopsis for inclusion in the Table of Contents.
SYNOPSIS (Word Style "SN_Synopsis_TOC"). If you are submitting your paper to a journal that requires a synopsis, see the journal's Instructions for Authors for details.